Simulation of Plasma Flow Injection with Multi-Hierarchy Model Aiming Magnetic Reconnection Studies

S. Usami[1,*], H. Ohtani[1,2], R. Horiuchi[1,2] and M. Den[3]

[1] *Department of Helical Plasma Research, National Institute for Fusion Science, Toki, 509-5292, Japan.*
[2] *The Graduate University for Advanced Studies (Soken-dai), Toki, 509-5292, Japan.*
[3] *National Institute of Information and Communications Technology, Koganei 184-8795, Japan.*

Abstract. A multi-hierarchy simulation model aiming magnetic reconnection studies is developed and improved in which macroscopic and microscopic physics are computed consistently and simultaneously. Macroscopic physics is solved by magnetohydrodynamics (MHD) algorithm, while microscopic dynamics is expressed by particle-in-cell (PIC) algorithm. The multi-hierarchy model relies on the domain decomposition method, and macro- and micro-hierarchies are interlocked smoothly by hand-shake scheme. As examination, plasma flow injection is simulated in the multi-hierarchy model. It is observed that plasmas flow from a macro-hierarchy to a micro-hierarchy across the magnetic field smoothly and continuously.

AMS subject classifications: 85D10, 93B40, 70B05, 76W05

Key words: Multi-hierarchy simulation, magnetic reconnection, MHD, PIC.

1 Introduction

Collisionless magnetic reconnection is one of the fundamental processes in which energy is converted from magnetic field energy to kinetic energy. It plays an essential role in the rapid energy release in laboratory fusion device and astrophysical plasmas [1–3]. Furthermore, of particular interest is an aspect of the coupling phenomenon between multiple spatial and temporal scales. When magnetic reconnection occurs, the field topology changes on a macroscopic scale and global plasma transport takes place. On the other

---

*Corresponding author. *Email addresses:* `usami.shunsuke@nifs.ac.jp` (S. Usami), `ohtani.hiroaki@nifs.ac.jp` (H. Ohtani), `horiuchi.ritoku@nifs.ac.jp` (R. Horiuchi), `den@nict.go.jp` (M. Den)

hand, an electrical resistivity controlled by a microscopic process is necessary as a trigger. A grand challenge is to understand a magnetic reconnection process as multi-hierarchy phenomenon completely [4].

Magnetohydrodynamics (MHD) simulations [5,6] is one of the popular tool for investigation of magnetic reconnection. However, the MHD algorithm assumes artificial electrical resistivity and viscosity, and can not describe their generation mechanism. On the other hand, fully kinetic electromagnetic particle-in-cell (PIC) simulations [7–10] treat dynamics of plasma by calculating motions of electrons and ions in the first principle, thus can express electrical resistivity and viscosity self-consistently [11–13]. However, the PIC algorithm requires huge computer resources in memory and CPU time, consequently large-scale simulation which deals with entire geomagnetosphere can not be executed. In order to conquer this problem, we develop a multi-hierarchy simulation model, which deals with both microscopic and macroscopic physics consistently and simultaneously as the MAgnetic Reconnection Interlocked Simulation (MARIS) project.

Recently we succeeded in the first demonstration of multi-hierarchy simulation in which plasma inflows come from the macroscopic domain and drive magnetic reconnection in the microscopic domain [14, 15]. Examining validity of our multi-hierarchy model was done in the previous work. In 2008, we simulated the propagation of Alfvén wave and observed that waves smoothly propagated in the multi-hierarchy simulation box [16, 17]. Now in this paper, in order to demonstrate validity of our model moreover, we simulate plasma flow injection in the multi-hierarchy model. This work plays a role to emphasize that magnetic reconnection phenomena found in the multi-hierarchy model as shown in [14, 15] exhibit true physics.

In Section 2, we describe the method of our multi-hierarchy simulation model for magnetic reconnection studies. The simulation domain is divided into three domains, and the macroscopic (MHD) and microscopic (PIC) domains are interlocked via the interface domain. Also, it is shown that the MHD and PIC algorithms have different time steps and how data are exchanged each other. In Section 3, we perform multi-hierarchy simulations of plasma injection. Plasmas are observed to smoothly and continuously flow in multi-hierarchy simulation box. In Section 4, we discuss a numerical error accumulated when thermal velocities are computed. Section 5 gives a summary of our work.

2 Multi-hierarchy simulation method

2.1 Multi-hierarchy structure of magnetic reconnection

In the multi-hierarchy structure of magnetic reconnection, the characteristic spatial and temporal scales are different by domains. In the vicinity of the reconnection point, phenomena are microscopic. For instance, the width of a current sheet and the gradient scale of magnetic field are of the order of ion gyroradius (strictly describing, the ion meandering scale). On the other hand, as being away from the reconnection point, phenomena relax to large-scale and slow behavior. As a result, plasma behavior can be expressed
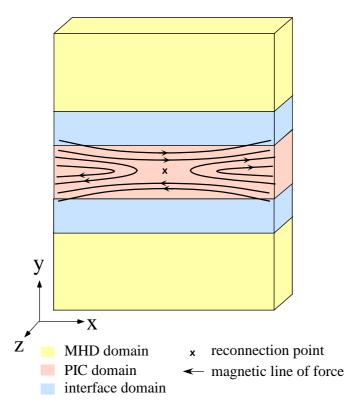
Figure 1: Schematic diagram of a multi-hierarchy model for magnetic reconnection simulation. Simulation domain is divided into three domains; MHD, PIC, and interface domains.

by one-fluid model in the domain enough more than the ion skin depth away from the reconnection point [18].

Based on the above features, the method that different algorithms are used in different domains is quite effective for magnetic reconnection studies. We refer to this method as domain decomposition method.

2.2   Domain decomposition method

Let us describe the domain decomposition method in detail. We show the schematic diagram of multi-hierarchy model for magnetic reconnection in Fig. 1. The simulation domain is divided into three domains, the MHD, PIC, and interface domain, and the MHD and PIC domains are connected via the interface domain in the upstream direction along y-axis. The MHD domain is a macro-hierarchy, and is taken to be the region far away from the reconnection point (the neutral sheet), namely the region outside the ion skin depth. In the MHD domain, MHD simulation method is used as calculation algorithm, since plasma dynamics in this domain is assumed to be expressed by one-fluid model. On the other hand, the PIC domain is a micro-hierarchy, and covers the central region. The physics in the PIC domain is calculated by PIC simulation method, since ki-

netic effects are supposed to play important roles. Between the MHD and PIC domains, an interface domain with a finite width is inserted. The physics in the interface domain is solved by both the PIC and MHD algorithms. Thus, MHD condition should be fully satisfied in the interface domain. In other word, the interface domain must be located fully outside the ion skin depth.

2.3 Hand-shake scheme

In order to interlock the PIC and MHD domains smoothly, an interconnection algorithm in the interface domain is crucial.

The governing equations in the MHD algorithm [19] are as follows:

$$\frac{\partial \rho}{\partial t} = -\nabla \cdot (\rho \boldsymbol{u}), \tag{2.1}$$

$$\frac{\partial (\rho \boldsymbol{u})}{\partial t} = -\nabla \cdot (\rho \boldsymbol{u} \boldsymbol{u}) - \nabla P + \frac{1}{4\pi} (\nabla \times \boldsymbol{B}) \times \boldsymbol{B}, \tag{2.2}$$

$$\frac{\partial \boldsymbol{B}}{\partial t} = \nabla \times (\boldsymbol{u} \times \boldsymbol{B}), \tag{2.3}$$

$$\frac{\partial P}{\partial t} = -\nabla \cdot (P \boldsymbol{u}) - (\Gamma - 1) P \nabla \cdot \boldsymbol{u}, \tag{2.4}$$

where ρ, $\boldsymbol{u}$, $\boldsymbol{B}$, P, and Γ denotes the mass density, fluid velocity, magnetic field, pressure, and ratio of specific heats. On the other hand, the basic equations in the PIC algorithm [20] are

$$\frac{1}{c} \frac{\partial \boldsymbol{B}}{\partial t} = -\nabla \times \boldsymbol{E}, \tag{2.5}$$

$$\frac{1}{c} \frac{\partial \boldsymbol{E}}{\partial t} = \nabla \times \boldsymbol{B} - \frac{4\pi}{c} \boldsymbol{J}, \tag{2.6}$$

$$\nabla \cdot \boldsymbol{B} = 0, \tag{2.7}$$

$$\nabla \cdot \boldsymbol{E} = 4\pi \rho_q, \tag{2.8}$$

$$\frac{d(\gamma_k \boldsymbol{v}_k)}{dt} = \frac{q_k}{m_k} \left(\boldsymbol{E} + \frac{\boldsymbol{v}_k}{c} \times \boldsymbol{B} \right), \tag{2.9}$$

$$\frac{d\boldsymbol{x}_k}{dt} = \boldsymbol{v}_k, \tag{2.10}$$

where $\boldsymbol{x}_k$, $\boldsymbol{v}_k$, m_k, q_k, and γ_k are the position, velocity, mass, charge, and Lorentz factor of the k-th particle, respectively and $\boldsymbol{E}$ is the electric field[†]. The current density $\boldsymbol{J}$ and charge

---

[†]We solve Eqs. (2.5) and (2.6) in Maxwell equations for $\boldsymbol{E}$ and $\boldsymbol{B}$, and $\boldsymbol{E}$ is adjusted by using the correction of the electrostatic part to satisfy Eq. (2.8). Eq. (2.7) always holds if it is initially satisfied.

density ρ_q are calculated by taking a sum over all the particles as,

$$J = \sum_{k=1}^{N} q_k v_k S(x - x_k), \tag{2.11}$$

$$\rho_q = \sum_{k=1}^{N} q_k S(x - x_k), \tag{2.12}$$

where N is total number of particles, and S is the form function of particles. We advance the simulation time by solving Eqs. (2.1)-(2.10). Physical quantities at the next time step $n+1$ can be expressed as a function of ones at the current time step n;

$$Q_l^{(n+1)} = G(Q_1^{(n)}, Q_2^{(n)}, Q_3^{(n)}, \cdots). \tag{2.13}$$

Here $Q_l^{(n)}$ is a physical quantity, the subscript l and superscript n represent the kind of quantities and the time step, respectively, and G is a function of known quantities $Q_l^{(n)}$‡.

At first, we consider macroscopic quantities such as electromagnetic field, fluid velocity, mass density, and pressure. In the MHD algorithm, macroscopic quantities are directly computed by Eqs. (2.1)-(2.4). On the other hand, the PIC algorithm calculates individual particle motions and does not directly treat the fluid velocity, mass density, and pressure. Hence, we obtain macroscopic quantities by assembling particle velocities and positions statistically based on the relations,

$$\rho = \sum_{k=1}^{N} m_k S(x - x_k), \tag{2.14}$$

$$\rho u = \sum_{k=1}^{N} m_k v_k S(x - x_k), \tag{2.15}$$

$$P = \frac{1}{3} \sum_{k=1}^{N} m_k (v_k - u)^2 S(x - x_k). \tag{2.16}$$

A macroscopic quantity in the interface domain $Q_{\text{interface}}$ is given by a hand-shake scheme [16,21];

$$Q_{\text{interface}} = F Q_{\text{MHD}} + (1 - F) Q_{\text{PIC}}. \tag{2.17}$$

The interconnection function F depends on the coordinates. The quantity Q_{MHD} is calculated by the MHD algorithm independently of the PIC algorithm and corresponds to the left-hand side of Eq. (2.13), while Q_{PIC} is solved by the PIC algorithm not using the MHD algorithm and corresponds the left-hand side of Eq. (2.13). After obtaining Q_{MHD}

---

‡In the strict sense, we employ the leap-flog method in the PIC algorithm, thus $Q_l^{(n+1/2)}$ is included in the right-hand side of Eq. (2.13). However, this fact does not affect an interconnection algorithm discussed below.

and Q_{PIC}, we have $Q_{\text{interface}}$ according to the hand-shake scheme (2.17). At the next time step, the obtained quantity $Q_{\text{interface}}$ is substituted in the right-hand side of Eq. (2.13).

However, an electric field E and current density J are treated exceptionally, since they are not independent variables in the MHD algorithm, in which E_{MHD} and J_{MHD} are given as

$$E_{\text{MHD}} = -u_{\text{MHD}} \times B_{\text{MHD}}, \tag{2.18}$$

and

$$J_{\text{MHD}} = \frac{1}{4\pi} \nabla \times B_{\text{MHD}}. \tag{2.19}$$

By using Eq. (2.17), $E_{\text{interface}}$ and $J_{\text{interface}}$ are obtained, however they are not used in Eq. (2.13) in the MHD algorithm, while they are substituted in the right-hand side of Eq. (2.13) in the PIC algorithm.

In order to solve the physics in the interface domain with the PIC algorithm, microscopic quantities such individual particle positions and velocities are needed. We assume that the (shifted) Maxwellian distribution is satisfied in the interface domain. At every PIC time step, particle velocities and positions in the interface domain are removed and newly determined so as to satisfy the profiles with the fluid velocity $u_{\text{interface}}$, mass density $\rho_{\text{interface}}$, pressure $P_{\text{interface}}$ (the thermal velocity $v_{T,\text{interface}}$, number density $n_{\text{interface}}$), and the current density $J_{\text{interface}}$. The new information of particle velocities and positions are substituted in the right-hand side of Eq. (2.13). After that, Eq. (2.13) goes forward one time step [the equations of motion (2.9) and (2.10) are solved] and particle velocities and positions at the next PIC time step are calculated.

2.4 Unit-transformation

Exchange of physical quantities between the MHD and PIC algorithms requires to transform unit, since normalization constants are different each other. Table 1 represents physical quantities and normalization constants in the MHD and PIC algorithms. For instance, velocities in the MHD algorithm are normalized to the Alfvén speed v_A, while ones in the PIC algorithm are normalized to the speed of light c.

We show the unit-transformation of physical quantities calculated by the PIC algorithm. First of all, we assume that normalization constant of magnetic field in the MHD algorithm equals to that of the PIC algorithm and define that MHD unit length is α times PIC unit length;

$$B_n = \frac{m_e^{\text{SP}} c \omega_{ce}}{q_e^{\text{SP}}}, \tag{2.20}$$

$$L = \alpha(c/\omega_{ce}), \tag{2.21}$$

where B_n is the normalization constant of magnetic field in the MHD algorithm and is arbitrary, m_e^{SP} is the electron super-particle mass, ω_{ce} is the electron gyrofrequency, q_e^{SP} is the

Table 1: Normalization constants in the MHD and PIC equations. Here, L, B_n, and ρ_n are arbitrary, c is the speed of light, ω_{ce} is the electron gyrofrequency, v_A is the Alfvén speed [$v_A = B_n(4\pi\rho_n)^{-1/2}$], m_e^{SP} is the electron super-particle mass, and q_e^{SP} is the electron super-particle charge.

	normalization constant	
Quantity	MHD	PIC
length	L	c/ω_{ce}
velocity	v_A	c
time	L/v_A	$1/\omega_{ce}$
magnetic field	B_n	$m_e^{SP}c\omega_{ce}/q_e^{SP}$
electric field	$v_A B_n$	$m_e^{SP}c\omega_{ce}/q_e^{SP}$
mass	-	m_e^{SP}
charge	-	q_e^{SP}
mass density	ρ_n	$m_e^{SP}(c/\omega_{ce})^{-3}$
pressure	$\rho_n v_A^2$	$m_e^{SP}c^2(c/\omega_{ce})^{-3}$
current density	$B_n/(4\pi L)$	$q_e^{SP}c(c/\omega_{ce})^{-3}$

electron super-particle charge, and L is arbitrary length. The parameter α can be determined freely. Furthermore, in particle simulations, the ion-to-electron mass ratio m_i/m_e is given, and the ratio of the electron plasma frequency to the electron gyrofrequency ω_{pe}/ω_{ce} is also taken to be certain value, which is satisfied at the standard electron number density n_{e0}. Therefore, we can transform PIC quantities in PIC unit system to those in MHD unit system as follows.

$$B_{\text{M-u}} = B_{\text{P-u}}, \tag{2.22}$$

$$E_{\text{M-u}} = \frac{\omega_{pe}}{\omega_{ce}}\sqrt{\frac{m_i}{m_e}}E_{\text{P-u}}, \tag{2.23}$$

$$r_{\text{M-u}} = \frac{1}{\alpha}r_{\text{P-u}}, \tag{2.24}$$

$$u_{\text{M-u}} = \frac{\omega_{pe}}{\omega_{ce}}\sqrt{\frac{m_i}{m_e}}\frac{m_e u_{e,\text{P-u}} + m_i u_{i,\text{P-u}}}{m_e + m_i}, \tag{2.25}$$

$$t_{\text{M-u}} = \frac{1}{\alpha}\frac{\omega_{ce}}{\omega_{pe}}\sqrt{\frac{m_e}{m_i}}t_{\text{P-u}}, \tag{2.26}$$

$$\rho_{\text{M-u}} = \frac{1}{n_{e0,\text{P-u}}}\frac{n_{e,\text{P-u}}m_e + n_{i,\text{P-u}}m_i}{m_i}, \tag{2.27}$$

$$P_{\text{M-u}} = \left(\frac{\omega_{pe}}{\omega_{ce}}\right)^2\frac{1}{n_{e0,\text{P-u}}}\frac{n_{e,\text{P-u}}m_e v_{Te,\text{P-u}}^2 + n_{i,\text{P-u}}m_i v_{Ti,\text{P-u}}^2}{m_e}, \tag{2.28}$$

$$J_{\text{M-u}} = \alpha\left(\frac{\omega_{pe}}{\omega_{ce}}\right)^2\frac{1}{n_{e0,\text{P-u}}}J_{\text{P-u}}, \tag{2.29}$$

where r, u_e, u_i, t, v_{Te}, and v_{Ti} denote the length, electron fluid velocity, ion fluid velocity, time, electron thermal velocity, and ion thermal velocity, respectively and the subscripts

M-u and P-u mean quantities normalized in MHD and PIC unit systems, respectively. Let us note that the quantities on the left-hand side have MHD unit, however they are data simulated by the PIC algorithm. In other words, quantities such as u_{M-u} and ρ_{M-u} correspond to Q_{PIC} in Eq. (2.17). As state above, after transformation from PIC to MHD unit systems, we operate the relation (2.17) in order to give macroscopic physical quantities in the interface domain.

On the other hand, for treating physics in the interface domain with the PIC algorithm, we transform $Q_{interface}$ in MHD unit system into $Q_{interface}$ in PIC unit system. Furthermore, for creating Maxwellian distribution in the PIC algorithm, fluid (averaged) velocities, thermal velocities, and number densities of electrons and ions in PIC unit system are needed. Thus, supposing electrons and ions have the same number density and temperature each other, we transform the fluid velocity, mass density and pressure in MHD unit system to the number densities, fluid (averaged) velocities, and thermal velocities of electron and ion in PIC unit system, respectively as follows.

$$n_{e,P-u} = n_{i,P-u} = n_{e0,P-u} \frac{m_i}{m_e + m_i} \rho_{M-u}, \tag{2.30}$$

$$u_{e,P-u} = \frac{\omega_{ce}}{\omega_{pe}} \sqrt{\frac{m_e}{m_i}} u_{M-u} - \frac{1}{\alpha} \left(\frac{\omega_{ce}}{\omega_{pe}} \right)^2 \frac{m_e + m_i}{m_i} \frac{J_{M-u}}{\rho_{M-u}}, \tag{2.31}$$

$$u_{i,P-u} = \frac{\omega_{ce}}{\omega_{pe}} \sqrt{\frac{m_e}{m_i}} u_{M-u}, \tag{2.32}$$

$$v_{Te,P-u}^2 = \frac{1}{2} \left(\frac{\omega_{ce}}{\omega_{pe}} \right)^2 \frac{m_e + m_i}{m_i} \frac{P_{M-u}}{\rho_{M-u}}, \tag{2.33}$$

$$v_{Ti,P-u}^2 = \frac{1}{2} \left(\frac{\omega_{ce}}{\omega_{pe}} \right)^2 \frac{m_e + m_i}{m_i} \frac{m_e}{m_i} \frac{P_{M-u}}{\rho_{M-u}}. \tag{2.34}$$

The electron fluid velocity is determined by Eq. (2.31), since the difference between ion and electron fluid velocities produces an electric current in the PIC algorithm.

2.5 Simulation time-flow

We show time-flow of our multi-hierarchy simulation in Fig. 2. We employ multi-time step scheme, where the MHD and PIC algorithms have different time steps each other. Large time steps are for the MHD algorithm, and small ones are for the PIC algorithm. For advancing time from t_1 to t_2, the PIC algorithm receives interpolation values of MHD data at t_1 and at t_2 from the MHD algorithm at every PIC time step. On the other hand, at t_1, the MHD algorithm gets PIC data averaged over several steps around t_1.

The following procedure makes time advance from t_1 to t_2.

Step 1: Supposing that at $t = t_1$, physical quantities of the MHD and PIC domains are given.

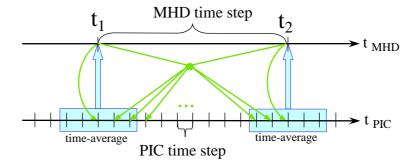Step 2: The MHD algorithm sends MHD information at t_1 to the PIC algorithm.

Figure 2: Time-flow of the multi-hierarchy simulation. The time steps for the MHD and PIC algorithms are different each other.

Step 3: The PIC algorithm sees MHD data at t_1 received in Step 2 as Q_{MHD} in Eq. (2.17) and advances to $t = t_1 + \delta t$, where δt is time which corresponds to several time steps of the PIC algorithm.

Step 4: PIC information averaged over the period from $t_1 - \delta t$ to $t_1 + \delta t$ is sent to the MHD algorithm.

Step 5: The MHD algorithm advances one time step and reaches t_2, referring to PIC data obtained in Step 4 as Q_{PIC} in Eq. (2.17).

Step 6: PIC information at $t = t_1 + \delta t$ which were obtained in Step 3 is removed and the PIC algorithm goes back to $t = t_1$.

Step 7: The MHD algorithm sends MHD data at t_1 and ones at t_2 to the PIC algorithm.

Step 8: During $t_1 < t < t_2$, the PIC algorithm refers to MHD data interpolated between at t_1 and at t_2 received in Step 7 as Q_{MHD} in Eq. (2.17) and advances to t_2.

3 Simulation results

Now we perform multi-hierarchy simulation of plasma injection from the MHD to PIC domains. Fig. 3 shows the schematic diagram of simulation box. This model is not configured for simulations of magnetic reconnection, hence, the following initial condition is given; the external magnetic field B_{x0} is taken to be x direction and the plasma mass density is uniform. The simulation box size is $4(c/\omega_{ce}) \times 176(c/\omega_{ce}) \times 1(c/\omega_{ce})$. The simulation domain is divided as follows. MHD domain: $0 < y/(c/\omega_{ce}) < 40$, $136 < y/(c/\omega_{ce}) < 176$, PIC domain: $48 < y/(c/\omega_{ce}) < 128$, interface domain: $40 < y/(c/\omega_{ce}) < 48$, $128 < y/(c/\omega_{ce}) < 136$. The system is periodic in x and z directions and is free in the y direction.

For plasma injection, an external electric field $E_{zd}(t)$ is applied at the entire outside boundary $[y/(c/\omega_{ce}) = 0, 176]$ of the MHD domain. According to ExB drift, plasmas flow inward in the y direction across the magnetic field. The electric field at the input boundary $E_{zd}(t)$ is programmed to evolve from zero to a constant value E_0. Here, E_0 is $0.06B_{x0}$ at $y/(c/\omega_{ce}) = 0$ and $-0.06B_{x0}$ at $y/(c/\omega_{ce}) = 176$ in PIC unit system.
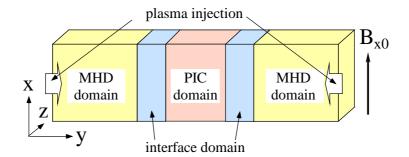
Figure 3: Schematic diagram of multi-hierarchy simulation box. Plasmas are injected from the MHD to PIC domains.
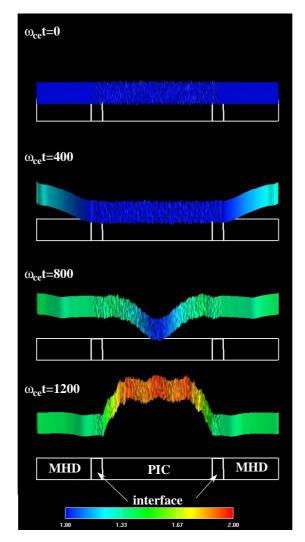

Figure 4: Bird's-eye view of plasma mass density ρ/ρ_0 at $\omega_{ce}t = 0$, 400, 800, and 1200. Here, ρ_0 is the initial mass density.

Simulation parameters are as follows. The ion-to-electron mass ration is $m_i/m_e=100$, and the ratio of the electron plasma frequency to the electron gyrofrequency is $\omega_{pe}/\omega_{ce}=1.0$. The grid spacings for the MHD and PIC algorithms are $\Delta r_{MHD}/L=\Delta r_{PIC}/(c/\omega_{ce})=0.25$. The parameter α in Eq. (2.21) is taken to be 1.0, thus Δr_{MHD} is equal to Δr_{PIC}. MHD time step is $\Delta t_{MHD}/(L/v_A)=0.1$ and PIC time step is $\Delta t_{PIC}\omega_{ce}=0.1$. Thus, 10 PIC time steps correspond to 1 MHD time step. As the interconnection function F, we use

$$F(y)=\frac{1}{2}\left(1+\cos\left[\pi\frac{y-y_{MHD}}{y_{PIC}-y_{MHD}}\right]\right), \tag{3.1}$$

where y_{MHD} and y_{PIC} are the boundary positions of the interface domain on the MHD and PIC sides, respectively [17]; $y_{MHD}/(c/\omega_{ce})=40, 136$ and $y_{PIC}/(c/\omega_{ce})=48, 128$. However, if we operate Eq. (3.1) for the thermal velocity (pressure), a numerical error would pile up. Then, we take

$$F(y)=\begin{cases}1, & (\text{for } y\neq y_{PIC}),\\ 0, & (\text{for } y=y_{PIC}),\end{cases} \tag{3.2}$$

only for the thermal velocity. In the Section 4, we will discuss why a different interconnection function is operated only for the thermal velocity (pressure).

Fig. 4 shows bird's-eye view of the mass density in the (y,x) plane at the various times. The mass density is normalized to the initial mass density ρ_0. At the initial state ($\omega_{ce}t=0$), mass density is uniform. In the early phase ($\omega_{ce}t\simeq400$), mass density increases in the MHD domain. At $\omega_{ce}t=800$ plasmas smoothly and continuously flow from the MHD to PIC domains through the interface domain, and at $\omega_{ce}t=1200$, mass density in the PIC domain reaches its maximum value $\rho/\rho_0=1.91$.

We can see that the mass density profile at $\omega_{ce}t=1200$ forms plateau structure. Using the momentum equation (2.2), the formation process of plateau structure is explained as follows. The force applied to plasma is mainly the gradient of magnetic pressure. Plasmas are carried inward by this force. In the early phase, there is pressure gradient in the MHD domain. At $\omega_{ce}t\simeq900$, leading plasmas collide at the center of the PIC domain. By that time, the electric field E_{zd} applied at the outside boundary of the MHD domain has already reached to a constant value. Thus, at $\omega_{ce}t\simeq900$ the magnetic pressure becomes to be nearly uniform. Plasmas however continue to move inward due to their inertia and accumulate at the center in the PIC domain. As a result, the magnetic pressure in the central region becomes to be higher, and thus following plasmas can not enter the central region and accumulate straight outside the high-pressure region so as to extend the high-pressure region. Therefore, plasma mass density profiles form plateau structure as shown in Fig. 4.

In these plasma injection phenomena, system spatial scale ($\sim 60c/\omega_{ce}$) is much larger than the ion gyroradius ($=2.5c/\omega_{ce}$) and temporal scale ($\sim 500/\omega_{ce}$) is also greater than the ion gyroperiod ($1/\omega_{ci}=100\omega_{ce}$). Therefore, these phenomena can be treated by the MHD framework. Let us compare results of the multi-hierarchy simulation with those of a MHD simulation, namely whole domain is calculated only with the MHD algorithm.
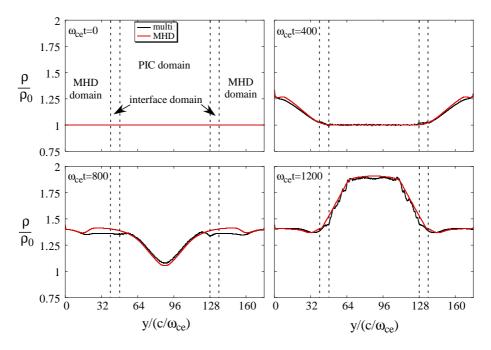
Figure 5: Spatial profiles of the plasma mass density ρ at $\omega_{ce}t$=0, 400, 800, 1200. Black and red lines represent results of the multi-hierarchy simulation and MHD simulation, respectively.
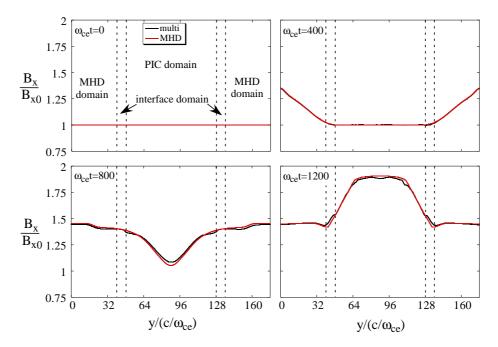

Figure 6: Spatial profiles of the magnetic field B_x for the same case as Fig. 5. Black and red lines represent results of the multi-hierarchy simulation and MHD simulation, respectively.

Table 2: Maximum of plasma mass density and width of its plateau for various $|E_0|$. Data with the multi-hierarchy and MHD simulations are listed for comparing.

	maximum ρ_{max}/ρ_0		width of plateau $h_p/(c/\omega_{ce})$	
$|E_0|/B_{x0}$	multi-hierarchy	MHD	multi-hierarchy	MHD
0.02	1.35	1.32	65	64
0.04	1.63	1.63	55	55
0.05	1.77	1.77	56	58
0.06	1.91	1.91	57	60
0.08	2.17	2.16	59	66

Fig. 5 shows spatial profiles of the mass density averaged in the x and z directions at the various times. Black and red lines denotes results of the multi-hierarchy simulation and MHD simulation, respectively. At $\omega_{ce}t = 0$, two lines are perfectly overlapped, so that black line is not seen. We can see that profiles of multi-hierarchy and MHD simulations are almost the same each other, though a profile in the multi-hierarchy simulation is a little different from one by MHD simulation around the interface domain at $\omega_{ce}t = 800$. Especially in the PIC domain, both the profiles and maximum values of mass density by the multi-hierarchy simulation fit well to those by the MHD simulation. Fig. 6 displays spatial profiles of the magnetic field for the same case as Fig. 5. We can see that the magnetic field also evolve in the similar way to the mass density, and is smoothly interlocked between the MHD and PIC domains.

In order to confirm the applicability of this scheme, we perform simulations in the cases of $|E_0|/B_{x0} = 0.02$, 0.04, 0.05, 0.06, and 0.08. It is observed that in the all cases plasmas smoothly and continuously move from the MHD and PIC domains, and consequently at $\omega_{ce}t \simeq 1200$ mass density profiles form plateau structure as shown in the bottom right panel of Fig. 5 and reach their maximum values. We investigate the maximum values of mass density ρ_{max} at $\omega_{ce}t = 1200$ and the width of mass density plateau h_p. Here the width of plateau is defined as the range where the mass density is larger than $0.9\rho_{max}$ at $\omega_{ce}t = 1200$. The results are listed in Table 2. Both the maximum of mass density and width of its plateau of the multi-hierarchy simulations are in agreement with those of MHD simulations. Our multi-hierarchy model can mimic a MHD model for plasma injection simulation. From these results, it is concluded that the interlocking method between the MHD and PIC domains (algorithms) is appropriate.

4 Discussion

In multi-hierarchy simulations in Section 3, Eq. (3.1) was not used as the interconnection function F only for thermal velocities. Why we have to use the function (3.2) comes from the character of the PIC algorithm. In general, when the PIC algorithm computes a thermal velocity by assembling particle velocities statistically, the value containing a numerical error $v_T(1+\delta)$ is obtained, where v_T is the exact thermal velocity and δ is a
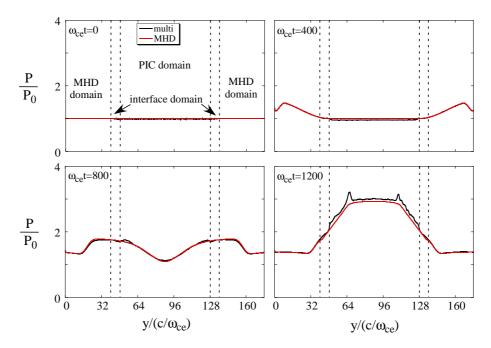
Figure 7: Spatial profiles of the plasma pressure P for the same case as Fig. 5. Here, P_0 is the initial pressure. Black and red lines represent results of the multi-hierarchy simulation and MHD simulation, respectively.

numerical error factor. If the numerical error has some tendencies, namely an averaged numerical error $<\delta>\neq0$, the error piles up.

Now it is supposed that particles have been distributed according to a Maxwellian distribution with a thermal velocity v_T. Let us consider a process that the PIC algorithm calculates a thermal velocity by assembling these particle velocities statistically, generates a Maxwellian distribution with a thermal velocity calculated, and again calculates a thermal velocity. At first, the PIC algorithm obtains $v_T(1+\delta)$ by assembling these particle velocities statistically, though the exact thermal velocity is v_T. Consequently, particles with a thermal velocity $v_T(1+\delta)$ are produced. Next, the PIC algorithm assembles these particle velocities statistically again, and would obtain $v_T(1+\delta)^2$. In general, δ is quite small. However, if the above process is done many times, the error would be accumulated so as to grow to large value.

Actually, in the multi-hierarchy simulations, all particles in the interface domain are removed and new particles satisfying Maxwellian distribution are put at every PIC time step. In the case when the interconnection function is Eq. (3.1), the numerical error of thermal velocity could grow, since a part of $v_{T,\text{PIC}}$ is included in $v_{T,\text{interface}}$. Therefore, we employ Eq. (3.2) as the interconnection function F only for thermal velocities.

In Fig. 7, we show profiles of the plasma pressure for the same case as Figs. 5 and 6. The pressure is continuously and smoothly connected through the interface domain. Its profiles of multi-hierarchy and MHD simulations fit fairly well each other, except there is a little difference in the PIC domain at $\omega_{ce}t=1200$.

Let us note the error growth of thermal velocity would occur in the case that a subroutine generates (shifted) Maxwellian distribution has the similar tendency.

5 Summary

For studies on magnetic reconnection process, we develop a multi-hierarchy simulation model based on the domain decomposition method. The simulation domain is divided into the MHD, PIC, and interface domains, and the domains differ in algorithms. Dynamics in the MHD and PIC domains are expressed by magnetohydrodynamics (MHD) and particle-in-cell (PIC) algorithms, respectively. The two domains are smoothly interlocked through the interface domain. The physics in the interface domain is calculated by both the MHD and PIC algorithms. The MHD and PIC algorithms have different time steps each other, however, the simulation time advances satisfying synchronism between the MHD and PIC algorithms.

We have simulated the injection of plasma flow by the multi-hierarchy model, which is not configured for magnetic reconnection, thus the initial magnetic field is uniform, but not anti-parallel. Plasmas are injected smoothly and continuously from the MHD to PIC domains via the interface domains. Also, comparing them with MHD simulations, we have confirmed that profiles of plasma mass density with the multi-hierarchy simulations fit those with MHD simulations well. This result clearly shows the adequacy for the multi-hierarchy simulation of magnetic reconnection which has demonstrated by the authors in recent year.

Acknowledgments

References

 [1] S. Masuda, T. Kosugi, H. Hara, S. Tsuneta, and Y. Ogawara, Nature 371 (1994) 495.
 [2] A. Nishida, Geophys. Res. Lett. 16 (1989) 227.
 [3] D. Biskamp, Magnetic Reconnection in Plasmas, Cambridge University Press, 2000.
 [4] R. Horiuchi, H. Ohtani, and A. Ishizawa, J. Plasma Phys. 72 (2006) 953.
 [5] R. Horiuchi and T. Sato, Phys. Fluids B1 (1989) 581.
 [6] M. Ugai, Phys. Plasmas 17 (2010) 032313.
 [7] W. Pei, R. Horiuchi, and T. Sato, Phys. Rev. Lett. 87 (2001) 235003.
 [8] R. Horiuchi, H. Ohtani, and A. Ishizawa, Comput. Phys. Commun. 164 (2004) 17.
 [9] B. Li and R. Horiuchi, Phys. Rev. Lett. 101 (2008) 215001.
[10] H. Ohtani and R. Horiuchi, Plasma Fusion Res. 4 (2009) 024.

[11] K. Nishimura, R. Horiuchi, and T. Sato, Phys. Plasmas 6 (1999) 3459.
[12] T. Moritaka, R. Horiuchi, and H. Ohtani, Phys. Plasmas 14 (2007) 102109.
[13] T. Moritaka and R. Horiuchi, Phys. Plasmas 15 (2008) 092114.
[14] S. Usami, H. Ohtani, R. Horiuchi, and M. Den, Plasma Fusion Res. 4 (2009) 049.
[15] R. Horiuchi, S. Usami, H. Ohtani, and T. Moritaka, Plasma Fusion Res. 5 Special Issue 2 (2010) S2006.
[16] S. Usami, H. Ohtani, R. Horiuchi, and M. Den, Commun. Comput. Phys. 4 (2008) 537.
[17] R. Horiuchi, S. Usami, H. Ohtani and M. Den, J. Plasma Fusion Res. SERIES 8 (2009) 184.
[18] A. Ishizawa and R. Horiuchi, Phys. Rev. Lett. 95 (2005) 045003.
[19] M. Scholer, J. Geophys. Res. 94 (1989) 8805.
[20] C. K. Birdsall and A. B. Langdon, Plasma Physics via Computer Simulation, McGraw-Hill, New York, 1985.
[21] T. Sugiyama and K. Kusano, J. Comput. Phys. 227 (2007) 1340.